

Bulletin of Pioneering Researches of Medical and Clinical Science

Available online: https://bprmcs.com 2021 | Volume 1 | Issue 1 | Page: 16-28

Fenofibrate Alleviates Neuroretinopathy in a Type 2 Diabetes Model Independently of Retinal Gene Activation via Peroxisome Proliferator-Activated Receptor Alpha

A. Kankanhalli¹, Alvin Chuen Wei Seah^{2*}, Seonghoon Kim³

¹ Duke-NUS Medical School, Singapore 169857, Singapore. ² Singapore Eye Research Institute, Singapore 169856, Singapore. ³ Institute of Molecular and Cell Biology, A*STAR, Singapore 138673, Singapore.

Abstract

Fenofibrate has been reported to slow diabetic retinopathy (DR), but the precise mechanisms in retinal tissue remain unclear. As an agonist of peroxisome proliferator-activated receptor alpha (PPARα), a key regulator of metabolism, inflammation, and oxidative stress, fenofibrate was hypothesized to protect against early retinal damage through PPARα activation. Using the db/db mouse model of type 2 diabetes, we found that six-month-old diabetic mice showed elevated blood lipids, reactive gliosis in the retina, and electroretinography (ERG) abnormalities, including diminished b-wave amplitudes and delayed oscillatory potentials, compared with nondiabetic littermates. Oral fenofibrate ameliorated these retinal dysfunctions. Surprisingly, fenofibrate did not trigger expression of PPARα target genes in either whole retina or isolated Müller glial cells. Further experiments using the PPARα agonist GW590735 in mice carrying a PPRE-luciferase reporter demonstrated robust activation in the liver but no detectable response in the retina. These results suggest that fenofibrate can limit early retinal pathology in type 2 diabetes through mechanisms independent of retinal PPARa activation.

Keywords: Müller Fenofibrate. Electroretinography, Diabetic retinopathy, PPAR-alpha

Corresponding author: Alvin Chuen Wei Seah E-mail: Alcinchuenweiseah@gmail.com

How to Cite This Article: Kankanhalli A, Wei Seah AC, Kim S. Fenofibrate Alleviates Neuroretinopathy in a Type 2 Diabetes Model Independently of Retinal Gene Activation via Peroxisome Proliferator-Activated Receptor Alpha. Bull Pioneer Res Med Clin Sci. 2021;1(1):16-28. https://doi.org/10.51847/pckF6V9Aoz

Introduction

Diabetes imposes a significant burden on retinal health, with diabetic retinopathy (DR) affecting over 4 million individuals and diabetic macular edema impacting more than 1 million people in the United States alone [1]. While treatments such as vascular endothelial growth factor (VEGF) inhibitors, corticosteroids, photocoagulation, and vitrectomy are available for visionthreatening disease, not all patients achieve a satisfactory response [2-4]. Consequently, there is a critical need for interventions that can slow disease progression before vision is compromised. Clinical trials, including the Fenofibrate Intervention and Event Lowering in Diabetes (FIELD) and Action to Control Cardiovascular Risk in Diabetes (ACCORD) studies, have demonstrated that fenofibrate can slow the advancement of mild to moderate non-proliferative DR and reduce the need for macular edema treatment [5, 6]. In cases of existing diabetic macular edema, combining fenofibrate with VEGF inhibitors yielded superior outcomes compared with VEGF inhibitors alone [7]. Despite these clinical benefits, the precise mechanisms by which fenofibrate exerts retinal protection remain unclear.

Experimental evidence supports a protective role of fenofibrate in animal models of DR. In db/db mice, a type 2 diabetes model, electroretinography (ERG) revealed decreased b-wave amplitudes at two and five months of age, which were partially restored with fenofibrate treatment. Similarly, in streptozotocin (STZ)-induced diabetic rats (a type 1 diabetes model), fenofibrate improved visual function assessed via the optokinetic (OKN) response [8-10]. These findings underscore the utility of animal models for investigating the molecular mechanisms underlying fenofibrate's retinal effects.

Fenofibrate is a known agonist of peroxisome proliferatoractivated receptor alpha (PPARα), a key regulator of lipid metabolism, inflammation, and oxidative stress. While PPARα activation in the liver mediates fenofibrate's lipidlowering effects, clinical improvements in DR occur independently of circulating lipid levels [5,6]. Evidence suggests that PPARa may also contribute directly to retinal health. In humans and rats, PPARα is expressed in Müller glial cells, with expression diminished under diabetic conditions [11]. Moreover, PPARa knockout mice exhibit retinal dysfunction, including reduced bwave amplitudes, capillary dropout, increased vascular leakage, elevated leukocyte adhesion, and higher levels of VEGF, tumor necrosis factor (TNF), and intracellular adhesion molecule (ICAM) [11, 12], which are exacerbated by STZ-induced diabetes [8]. Protective effects of fenofibrate in experimental models, such as reduced pericyte loss, decreased capillary dropout, and suppression of inflammatory mediators (VEGF, ICAM), appear dependent on PPARa and are lost in whole-body PPARα knockout mice [13-15]. These observations raise the possibility that fenofibrate may act as a PPARα agonist within the retina, exerting lipid-independent therapeutic effects.

The specific retinal cell types targeted by fenofibrate remain to be fully determined. The retina contains diverse neuronal, glial, and vascular cells, with rod photoreceptors representing roughly 80% of retinal cells in mice and rats. As a result, analyses of whole retinal tissue (e.g., Western blot, qPCR) predominantly reflect changes in rods. However, other cell types, particularly Müller glia, play essential roles in retinal metabolism, express PPARa under basal conditions, and respond to stressors, including diabetes, through gliosis [16-19]. Fenofibrate can reverse Müller glial gliosis and restore expression of key transporters such as GLAST in db/db mice [10]. In STZinduced diabetic mice, Müller glia upregulate oxidative stress response genes (Nrf2, Nqo-1, Ho-1, Sod1), and fenofibrate further enhances this response while suppressing the nlrp3 inflammasome, IL-1β, and caspase1 [10]. These findings indicate Müller glia as likely direct targets of fenofibrate in the retina.

In this study, we further examined the protective effects of fenofibrate in db/db mice, focusing on retinal metabolism, gliosis, and ERG changes. We also tested the hypothesis that fenofibrate functions as a PPAR α agonist within the retina and Müller glia by profiling global retinal gene expression following oral or intravitreal fenofibrate administration, evaluating PPAR α target gene expression in Müller glia, and assessing retinal responsiveness to PPAR α activation using a luciferase reporter assay.

Materials and Methods

Animal models

All experimental procedures, including euthanasia, adhered to the NIH Guide for the Care and Use of Laboratory Animals and were approved by the Washington University in St. Louis IACUC (Protocol #19-0950). The study utilized the following mouse strains: C57BL/6J (Jackson Laboratory, Stock #00664), BKS.Cg-Dock7m +/+ Leprdb/J ("db/db," Stock #00642), Tg(Slc1a3-cre/ERT)1Nat/J ("GLAST-CreER," B6.Cg-Gt(ROSA)26Sortm14(CAG-#012586), and tdTomato)Hze/J ("tdTomato," Stock #007914) [20-22]. For in vivo reporter studies, a peroxisome proliferator response element luciferase transgenic line on a C57BL/6J background (repTOP PPRE-Luc, Charles River) was employed [23, 24]. After weaning, mice were fed standard chow until 3 months of age, after which they were either maintained on this diet or switched to chow supplemented with 0.2% w/w fenofibrate (custom-milled, Envigo Teklad) [25].

Metabolic assessments

Prior to sample collection, animals were fasted for six hours on hardwood bedding. Blood from the tail vein was collected to determine glucose levels using Sigma Pharmaceuticals reagents (North Liberty, IA, USA). Triglycerides and cholesterol were measured using Thermo Fisher Scientific kits (Waltham, MA, USA), and free fatty acids (FFAs) were assessed using Wako reagents (FUJIFILM Wako Chemicals, Richmond, VA, USA). For liver and retinal cholesterol content, tissues were weighed, homogenized in chloroform:methanol (2:1 v/v), and centrifuged at $13,400 \times g$ for 10 minutes at 4 °C. From the upper phase, 100 µL was dried at room temperature for 30 minutes, then incubated with 100 µL of Infinity Total Cholesterol reagent (Thermo Fisher Scientific, cat# TR13421) for 30 minutes. Absorbance at 490 nm was recorded, and absolute cholesterol concentrations were calculated against a standard curve and normalized to tissue weight.

Electroretinography (ERG)

ERG recordings were performed at six months of age using the UTAS BigShot System (LKC Technologies, Gaithersburg, MD, USA) [26]. Mice were dark-adapted overnight and anesthetized with ketamine (80 mg/kg) and xylazine (15 mg/kg). Pupils were dilated with 1% atropine sulfate. Full-field white light flashes (10 µs) were delivered under dark-adapted conditions or with a dim background (30 cd/m²). Each stimulus was repeated 10 times for low-intensity flashes and 5 times for brighter flashes, and responses were averaged across trials. Using MATLAB (MathWorks, Natick, MA, USA), the a-wave amplitude was defined from baseline to the most negative point, while the b-wave was measured from this point to the maximum positive peak after subtraction of oscillatory potentials (OPs), which were isolated with a 25 Hz highpass digital Butterworth filter. The eye with the larger bwave was used for analysis. Stimulus luminance was determined using manufacturer calibrations.

Immunohistochemistry

Eyes were collected from euthanized mice and fixed in 4% paraformaldehyde overnight. Following fixation, tissues were dehydrated, cryoprotected in sucrose, and embedded in optimal cutting temperature (OCT) medium. Using a Shandon Cryotome E cryostat, 15 µm-thick sections encompassing the optic nerve head were prepared. Sections were treated with 0.5% Triton X-100 in PBS to permeabilize the tissue and then incubated at 4°C overnight with primary rabbit antibodies against glial fibrillary acidic protein (GFAP; Agilent Technologies, Santa Clara, CA, USA, catalog #Z033429-2) diluted 1:500 in 10% donkey serum with 0.5% Triton X-100/PBS. After washing in PBS, sections were incubated with Alexa Fluor 594-conjugated secondary antibodies (Thermo Fisher Scientific, Waltham, MA, USA) under the same conditions. Sections were mounted in DAPI-containing fluorescence mounting medium (Dako, Technologies, Santa Clara, CA, USA). Imaging was performed using a Nikon Eclipse Ti inverted microscope (Nikon, Minato City, Tokyo, Japan) equipped with an LED light source (Lumencor, Beaverton, OR, USA) and a 40× (N.A. 1.4) objective, and images were processed with NIS-Elements software. Fluorescence intensity measurements were performed in ImageJ (NIH, Bethesda, MD, USA) and final figure preparation was done in Adobe Illustrator (Adobe Inc., San Jose, CA, USA).

Gene expression analysis in fenofibrate-treated mice Retinas were isolated from eight 6-month-old C57BL/6J mice fed a diet supplemented with fenofibrate and eight age-matched littermate controls (balanced for sex: four males, four females per group). Total RNA was extracted using Trizol, quantified using a Qubit fluorometer, and RNA integrity was assessed with an Agilent 2100 Bioanalyzer RNA nano chip (Agilent Technologies, Santa

Clara, CA, USA). For library preparation, 1 µg of RNA was used, and ribosomal RNA was depleted using the Ribo-Zero kit (Illumina, San Diego, CA, USA). Efficiency of rRNA removal and mRNA yield were checked via the Bioanalyzer. Messenger RNA was fragmented at 94 °C for 150 s in a buffer containing 40 mM Tris-Acetate (pH 8.2), 100 mM Potassium Acetate, and 30 mM Magnesium Acetate, then reverse-transcribed to cDNA using SuperScript III reverse transcriptase (Life Technologies, Carlsbad, CA, USA) with random hexamer primers. Double-stranded cDNA was synthesized, blunt-ended, Atailed at the 3' ends, and ligated with Illumina sequencing adapters. The resulting fragments were PCR-amplified for 12-15 cycles using indexed primers. Libraries were quantified by Qubit and evaluated with the Agilent TapeStation (Agilent Technologies, Santa Clara, CA, USA). Indexed libraries were pooled in equimolar amounts and sequenced on an Illumina HiSeq-3000 generating 50-base single-end reads (Illumina, San Diego, CA, USA).

Sequence data were demultiplexed using Illumina bcl2fastq and a custom Python script allowing one index mismatch. Reads were aligned to the Ensembl release 76 reference genome using STAR v2.0.4b [27], and genelevel counts were calculated with Subread:featureCount v1.4.5 [28] using uniquely mapped reads. Quality metrics, including total aligned reads, unique alignment fraction, ribosomal content, junction saturation, and read distribution over gene models, were assessed with RSeQC v2.3 [29].

Gene counts were normalized in R/Bioconductor using the DESeq package [30] with trimmed mean of M-values (TMM) factors to account for library size differences. Genes with zero expression across all samples were removed. Differential expression analysis was performed between fenofibrate-treated and control groups, retaining only genes with a Benjamini–Hochberg adjusted false discovery rate ≤ 0.05 .

Intravitreous injection and microarray profiling

Twelve male C57BL/6J mice, three months old, were anesthetized with ketamine (80 mg/kg body weight) and xylazine (15 mg/kg lean body mass). Mice were divided into four groups of three, and each received bilateral intravitreal injections as follows: 1 µL of fenofibrate (250 µM in 50 percent DMSO/normal saline), 1 µL of GW590735 (500 nM in 50 percent DMSO/NS), 1 µL of WY14643 (60 µM in 50 percent DMSO/NS), or 1 µL of 50 percent DMSO/NS as a vehicle control [15, 31]. Injections were administered using a 32-gauge needle inserted from the dorsal side of the eye just behind the limbus, taking care to avoid the lens. Following the procedure, a topical antibiotic ointment was applied, and mice were allowed to recover on a warming pad.

After 24 hours, mice were euthanized, and retinas were collected. Retinas from each animal were pooled, and RNA extraction was performed using Trizol. RNA integrity was verified with an Agilent 2100 Bioanalyzer (Total RNA nano chip, Agilent Technologies, Santa Clara, CA, USA), with all samples showing RIN values above 8.0. Amplified cDNA libraries were generated using the NuGEN Ovation PicoSL kit (NuGEN Technologies, Redwood City, CA, USA) and subsequently hybridized to Affymetrix GeneChip Mouse Gene 2.0 ST arrays (Affymetrix, Santa Clara, CA, USA). Array signals were processed and analyzed using Affymetrix Expression Console software.

Isolation and expression profiling of müller glia
To induce transgene activation, GLAST-CreER+;
R26CL:tdTomato fl/fl mice and GLAST-CreER(-/-);
R26CL:tdTomato fl/fl littermates received intraperitoneal injections of tamoxifen (Sigma-Aldrich, St. Louis, MO, USA) at 1–2 mg/day for five consecutive days when aged 1–2 months. Tamoxifen was prepared by dissolving in ethanol and diluting in sunflower oil to a final concentration of 20 mg/mL.

At six months, retinas were harvested, and Müller glia were isolated using fluorescence-activated cell sorting (FACS), as previously described [32]. Retinas were first placed in calcium- and magnesium-free PBS and enzymatically dissociated with 1 mg/mL trypsin (Sigma-Aldrich) combined with gentle mechanical trituration. Trypsin activity was then neutralized with 1 mg/mL trypsin inhibitor, and DNase I was applied to minimize cell clumping. Cells exhibiting tdTomato fluorescence were sorted using the PE-A channel on a FACS Aria II instrument (BD Biosciences, San Jose, CA, USA).

RNA from sorted cells was purified using the RNeasy Micro Kit (QIAGEN, Venlo, The Netherlands) and stored at $-80\,^{\circ}$ C until analysis. Reverse transcription was performed with Superscript II (Invitrogen, Carlsbad, CA, USA) according to the manufacturer's instructions on a Bio-Rad thermocycler. Gene expression was quantified by real-time PCR using a StepOnePlus system (Thermo Fisher Scientific, Waltham, MA, USA) with SYBR Green chemistry and primers listed in **Table 1**, with each sample analyzed in duplicate. Statistical differences were evaluated using unpaired Student's t-tests in Microsoft Excel (Microsoft, Redmond, WA, USA).

Table 1. qPCR primer sequences	
Primer	Sequence
Mm_rho_f1	CTCTGCCAGCTTTCTTTGCT
Mm_rho_r1	GTCGTCATCTCCCAGTGGAT
Mm_GS_f1	CTGCCATACCAACTTCAGCA
Mm_GS_r1	TGTGGTACTGGTGCCTCTTG
Mm Cptla fl	TGGGAGAGAATTTCATCCACTT
Mm_Cptla_rl	TCCATCATGGCTTGTCTCAA
Mm_Acox1_f1	GATGTGACCCTTGGCTCTGT
Mm Acox1 r1	GACTGCAGGGGCTTCAAGT
Mm_Acadm_f1	AGCTCTAGACGAAGCCACGA
Mm Acadm r1	GCGAGCAGAAATGAAACTCC
Mm_GAPDH_f1	TGCACCACCAACTGCTTAGC
Mm_GAPDH_r1	GGCATGGACTGTGGTCATGAG
Mm_L32_f1	TTCCTGGTCCACAATGTCAA
Mm_L32_r1	GGCTTTTCGGTTCTTAGAGGA

Luciferase reporter assay

PPRE-luciferase transgenic mice [23, 24] were treated at three months of age with either intraperitoneal injections of GW590735 (10 mg/kg) or intravitreal injections of 2 µL of GW590735 (500 nM). Twenty-four hours post-treatment, retinas and livers were collected for luciferase activity measurements. Tissues were first weighed and rinsed in PBS, and 10 mg of each sample (wet weight) was homogenized in 0.5 mL of passive lysis buffer (PLB; Promega, catalog #194A1) for 15 minutes. Following low-speed centrifugation to remove cellular debris, 10 µL of the supernatant was combined with 50 µL of assay buffer containing D-luciferin. Luminescence was quantified using a Turner TD-20/20 luminometer, capturing signals for both firefly and Renilla luciferases. Background signals from Renilla were subtracted from firefly readings

to correct for nonspecific luminescence, and all values were expressed relative to vehicle-treated controls.

Statistical procedures

For electroretinography measurements, response values at different light intensities were reported as mean \pm SEM. Each experimental group included at least three animals, with larger numbers specified in figure legends. Group comparisons were conducted using GraphPad Prism 6. Depending on the analysis, ordinary two-way ANOVA, one-way ANOVA, or unpaired Student's t-test was employed, with Bonferroni corrections applied for multiple comparisons where appropriate. Statistical significance was set at p < 0.05.

Results

Fenofibrate modulates lipid metabolism in db/db mice

To examine fenofibrate's metabolic effects, db/db mice, which carry a leptin receptor mutation and develop obesity, hyperglycemia, and dyslipidemia—especially under high-fat diet conditions—were used as a type 2 diabetes model [22, 33]. These pathophysiological features closely resemble human type 2 diabetes. At three months of age, db/db mice and their heterozygous db/+

littermates were randomly assigned to receive either standard chow or chow supplemented with 0.2% w/w fenofibrate for three months. Baseline assessment confirmed that db/db mice were heavier and had higher serum glucose levels than db/+ littermates (Table 2). No initial differences in these parameters were detected between mice allocated to fenofibrate versus standard chow diets.

Table 2. Metabolic parameters of fenofibrate-treated mice in a type 2 diabetes model								
Parameter	Non-Diabetic (db/m)		Diabetic (db/db)					
	Vehicle	Fenofibrate	Vehicle	Fenofibrate				
n	10	8	10	10				
Body weight (g) at 3 months, randomization	23.0 ± 1.2	24.8 ± 1.4	49.7 ± 1.1 ****	51.2 ± 2.1 ****				
Body weight (g) at 6 months, at assay	28.3 ± 1.3	25.5 ± 0.7	57.0 ± 2.4 ****	62.6 ± 0.9 ****				
Plasma glucose (mg/dL) at 3 months	121.0 ± 6.8	121.8 ± 8.8	421.4 ± 29.9 ****	445.3 ± 28.1 ****				
Plasma glucose (mg/dL) at 6 months	208.8 ± 9.1	179.5 ± 8.1	536.2 ± 33.8 ****	540.1 ± 32.9 ****				
Plasma triglycerides (mg/dL) at 6 months	46.0 ± 1.4	55.3 ± 5.1	71.7 ± 4.5 ****	$49.2 \pm 2.2 \# \# \# \#$				
Plasma free fatty acids (mM) at 6 months	0.81 ± 0.04	1.06 ± 0.09	1.46 ± 0.04 ****	1.34 ± 0.07 *				
Plasma cholesterol (mg/dL) at 6 months	49.6 ± 1.6	84 2 + 5 7 ##	103 2 + 5 9 ****	1276+90*** #				

Metabolic measurements for db/db and db/+ mice are presented at baseline (three months of age) and at 6 months following three months on either standard chow or a diet supplemented with fenofibrate. As expected, db/db mice displayed higher body weight and plasma glucose levels compared with their littermate controls at both time points, and these parameters were not altered by fenofibrate treatment. Plasma levels of triglycerides, free fatty acids, and cholesterol at six months are also reported. Statistical significance is indicated as follows: *p < 0.05, ***p < 0.001, ****p < 0.0001, based on two-way ANOVA comparing each group to healthy controls within the same dietary treatment; *p < 0.05, **p < 0.01, ***p < 0.0001, based on two-way ANOVA comparing each group to genotype-matched mice receiving the alternate diet.

At six months, following three months of dietary intervention, additional metabolic assessments were performed. At this stage, db/db mice continued to exhibit higher body weight and elevated serum glucose compared with their littermate controls, independent of fenofibrate treatment. Plasma triglyceride levels were significantly increased in db/db mice maintained on standard chow, but this rise was prevented in db/db mice receiving fenofibrate. Free fatty acid levels were also higher in db/db mice, and although fenofibrate supplementation did not produce a statistically significant reduction, there was a tendency toward lower levels compared with untreated db/db mice. Plasma cholesterol concentrations were elevated in db/db mice relative to controls, and fenofibrate

further increased cholesterol in both db/db and db/+ animals.

To investigate the source of the fenofibrate-induced increase in serum cholesterol, cholesterol content was measured in the liver and retina (Table 3). Liver cholesterol was higher in db/db mice compared with littermates but was not affected by fenofibrate supplementation in either genotype. Retinal cholesterol levels remained unchanged regardless of genotype or fenofibrate treatment. These results indicate that, while fenofibrate raises circulating cholesterol, it does not alter cholesterol content within the liver or retina in either db/db or wild-type mice.

Table 3. Tissue lipid content of fenofibrate-treated mice in a model of type 2 diabetes							
	Non-Diabetic db/m		Diabetic db/db				
	Vehicle	Fenofibrate	Vehicle	Fenofibrate			
n	3	3	3	3			
Liver Cholesterol Content (mg/dL/g tissue) 6 months	0.158 (0.016)	0.15 (0.005)	0.238 (0.015) *	0.255 (0.017) **			
Retinal Cholesterol Content (mg/dL/g tissue) 6	0.123 (0.004)	0.145 (0.013)	0.137 (0.006)	0.127 (0.012)			

At 3 months of age, db/db and db/+ mice were assigned to either a fenofibrate-supplemented diet or a standard chow diet. By six months, cholesterol content in the liver and retina was assessed. Liver cholesterol remained elevated in db/db mice regardless of dietary treatment, whereas retinal cholesterol levels showed no differences across genotypes or treatments. Statistical significance is indicated as *p < 0.05 and **p < 0.01, determined by two-way ANOVA compared to healthy controls within the same diet group.

Oral fenofibrate mitigates diabetes-induced reactive retinal gliosis

Reactive gliosis in the retina, a hallmark response of Müller glia to inflammatory or ischemic insults including diabetic retinopathy, involves hypertrophy of glial processes and upregulation of glial fibrillary acidic protein (GFAP). Immunohistochemical analysis of GFAP revealed pronounced gliosis in six-month-old db/db mice

compared with their db/+ littermates (Figure 1A, B). In contrast, db/db mice fed a fenofibrate-enriched diet displayed markedly reduced gliosis (Figure 1C). Across

all experimental groups, overall retinal architecture remained intact, as confirmed by DAPI nuclear staining (Figure 1D–F).

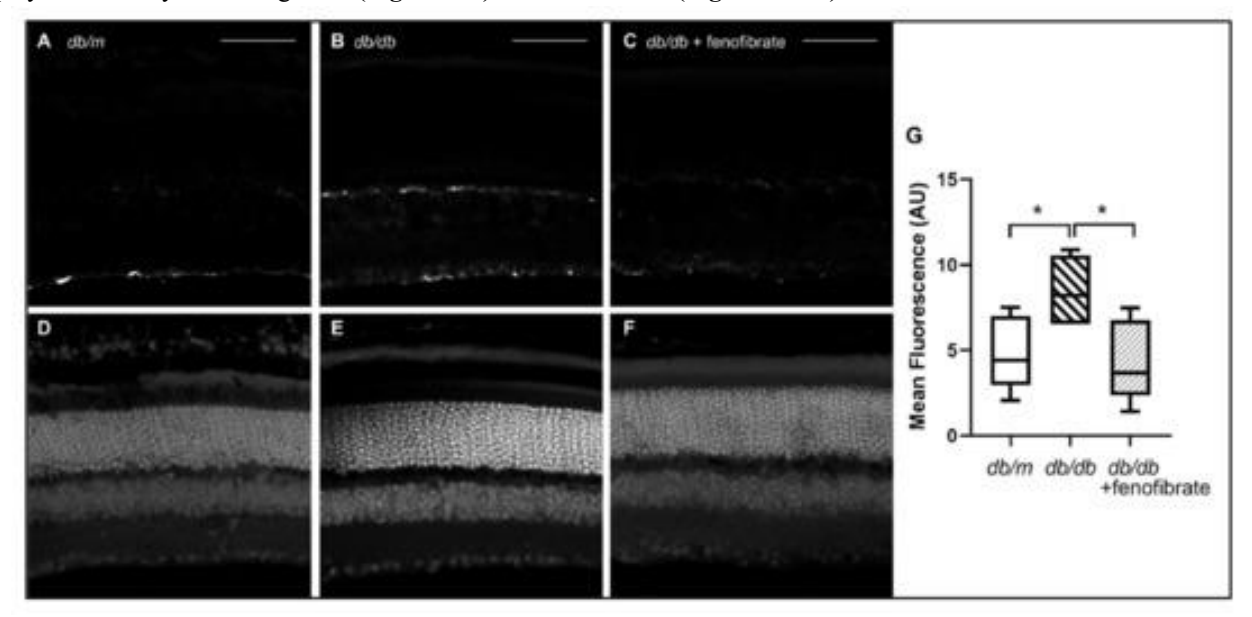


Figure 1. Fenofibrate Reduces Diabetes-Associated Reactive Retinal Gliosis

Retinas from six-month-old db/db mice and their heterozygous db/+ littermates were collected, fixed, sectioned, and stained for glial fibrillary acidic protein (GFAP) and DAPI. (A) In db/+ mice, GFAP staining was minimal and largely confined to the internal limiting membrane. (B) Diabetic db/db mice exhibited pronounced gliosis, with GFAP signal extending into the inner nuclear layer (INL). (C) Administration of oral fenofibrate to db/db mice markedly reduced gliosis, restoring GFAP staining patterns comparable to those observed in db/+ controls. (D–F) DAPI counterstaining confirmed intact nuclear morphology across groups. Scale bars: $50 \,\mu\text{m}$. (G) Relative fluorescence intensity was quantified for each group (n = 6 per group), with *p < 0.05 determined by one-way ANOVA.

Fenofibrate mitigates diabetes-related alterations in electroretinography

Retinal function in six-month-old db/db and db/+ mice evaluated using electroretinography (ERG), measuring oscillatory potential (OP) implicit times as well as a-wave and b-wave amplitudes under dark-adapted conditions. OP implicit time, indicative of inner retinal function and primarily influenced by amacrine cells, was delayed in db/db mice compared with their littermates (Figure 2A). Fenofibrate treatment partially corrected this OP delay in db/db animals. Similarly, b-wave amplitudes were reduced in db/db mice on standard chow but were preserved in those receiving fenofibrate supplementation (Figure 2B). While a-wave amplitudes were diminished at certain light intensities in db/db mice regardless of treatment, maximal a-wave amplitudes were comparable across all groups (Figure 2C, D). Collectively, these findings suggest that fenofibrate can alleviate diabetesinduced inner retinal dysfunction, potentially through effects on amacrine cell activity, whereas outer retinal function appears largely unaffected at this stage.

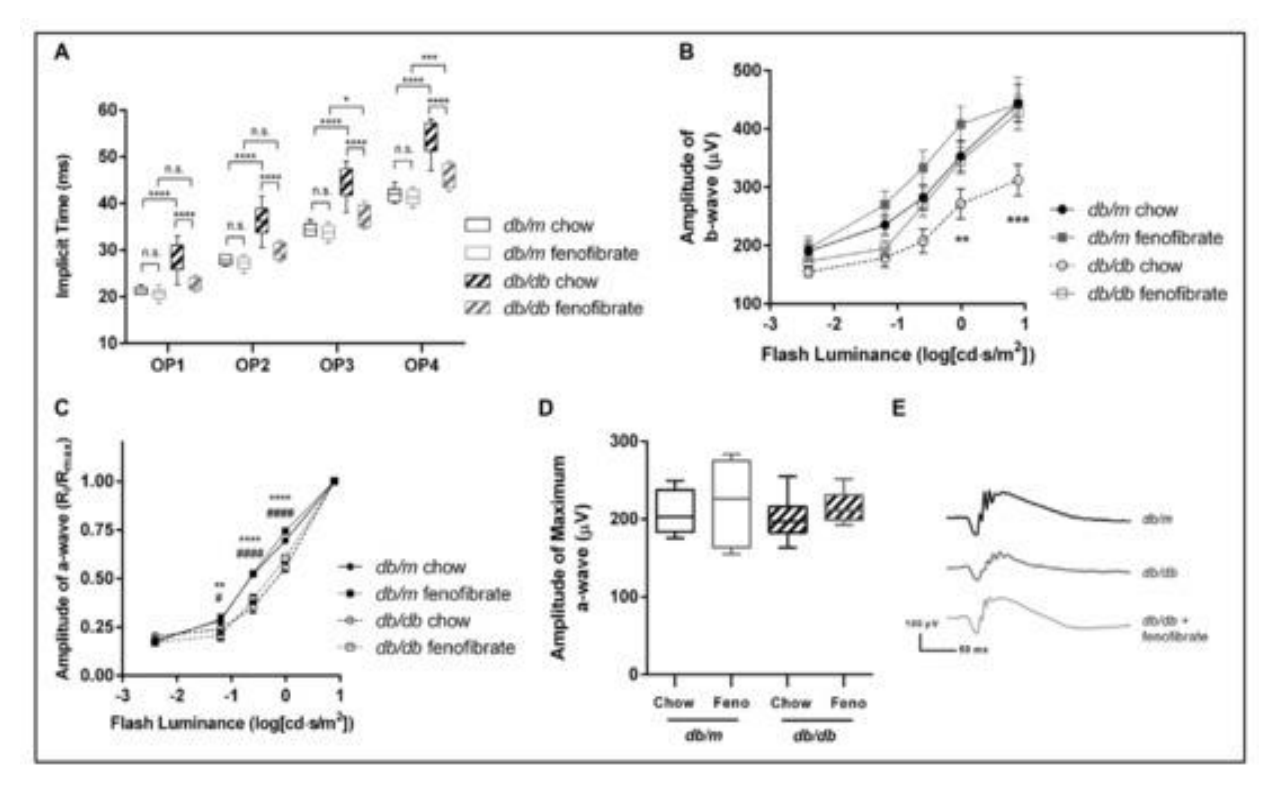


Figure 2. Fenofibrate Mitigates Diabetes-Associated Retinal Dysfunction in ERG

At six months, db/db mice and their heterozygous db/+ littermates were maintained on either standard chow or a diet supplemented with fenofibrate and evaluated via electroretinography (ERG). Analysis of the first four oscillatory potentials (OP1-OP4) revealed that untreated db/db mice exhibited notable delays relative to db/+ controls, whereas fenofibrate treatment partially restored normal OP timing in diabetic animals (Figure 2A). Measurement of b-wave amplitudes across varying flash intensities showed a reduction at higher luminances in db/db mice on regular chow, a deficit that was prevented in fenofibrate-supplemented db/db mice (Figure 2B). Awave amplitudes displayed minor reductions at certain flash intensities in db/db mice regardless of diet, but peak a-wave amplitudes were comparable across all groups (Figure 2C, D). Representative scotopic ERG traces in response to -0.01 log(cd·s/m²) flashes are presented in Figure 2E. Sample size per group was n = 10. Statistical significance was determined by two-way ANOVA, with comparisons to healthy controls within the same diet indicated by *p < 0.05, **p < 0.01, ***p < 0.001, ****p < 0.0001, and comparisons to genotype-matched mice on the alternate diet denoted by #p < 0.05, ###p < 0.0001.

Fenofibrate does not significantly alter retinal ppara gene expression in non-diabetic mice

Given the metabolic, structural, and functional changes observed in diabetic mice treated with fenofibrate, we examined whether oral fenofibrate affects retinal gene expression in non-diabetic animals. Whole retinas were collected from six-month-old C57BL/6J mice maintained on standard chow or fenofibrate-supplemented diets. RNA was extracted and subjected to high-throughput sequencing for genome-wide expression analysis. Overall transcriptomic profiles were nearly identical between the two dietary groups, with no genes reaching statistical significance after multiple testing correction (Figure 3A). Since fenofibrate is a known PPARα agonist, we specifically assessed genes annotated within the PPAR pathway according to KEGG. No meaningful changes were observed in this gene subset either (Figure 3B), indicating that fenofibrate does not substantially alter PPARα target expression in the retina of healthy mice.

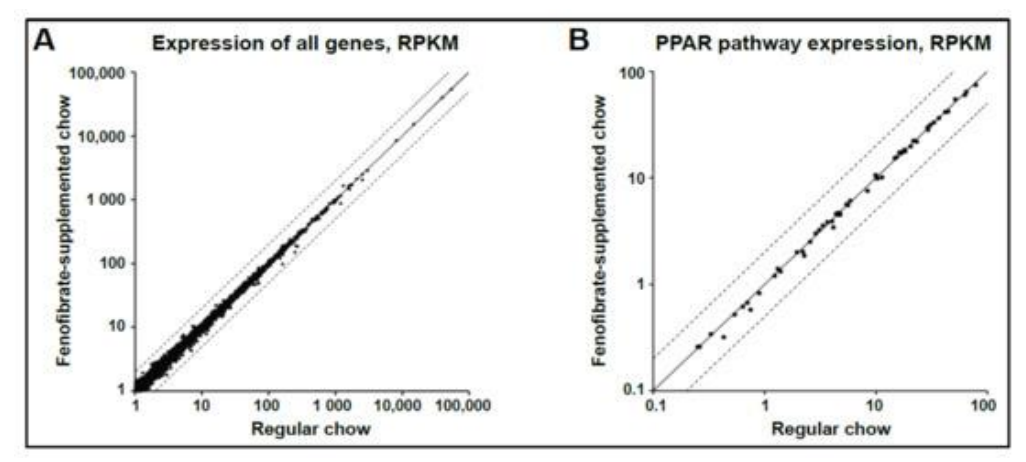


Figure 3. Whole-Retina Gene Expression Is Unaltered by Fenofibrate Diet

Mice were maintained on either a fenofibrate-supplemented or standard chow diet starting at one month of age, with four males and four females per group, and retinas were collected at six months. RNA was extracted from whole retinas and analyzed via RNA sequencing. Each data point represents the normalized expression of an individual gene in reads per kilobase per million mapped reads (RPKM). The solid diagonal line indicates equivalent expression between groups, whereas the dashed lines indicate a two-fold change in expression. (A) Global gene expression across all transcripts. (B) Expression of genes annotated in the PPAR pathway according to KEGG.

Local intravitreous fenofibrate does not modify retinal ppara target expression in non-diabetic mice To determine whether direct retinal exposure to fenofibrate could more effectively modulate gene

expression, three-month-old male mice received intravitreous injections of fenofibrate (1 μL, 250 μM) or vehicle (1 μL, 50:50 DMSO/normal saline). Retinas were harvested 24 hours later, and RNA was isolated for global transcriptomic analysis using microarrays. Consistent with the oral supplementation data, retinal gene expression was largely unchanged between fenofibrate- and vehicletreated animals, with no significant differences after correction for multiple comparisons (Figure 4A). Genes specifically associated with the PPAR pathway, as annotated by KEGG, also showed stable expression (Figure 4D). Two additional PPARα agonists, GW590735 (1 μL, 500 nM) and WY14643 (1 μL, 60 μM), were included as positive controls via intravitreal injection. Microarray analysis revealed minimal changes in global gene expression, and PPAR pathway genes in particular remained largely unaltered (Figure 4B,C,E,F).

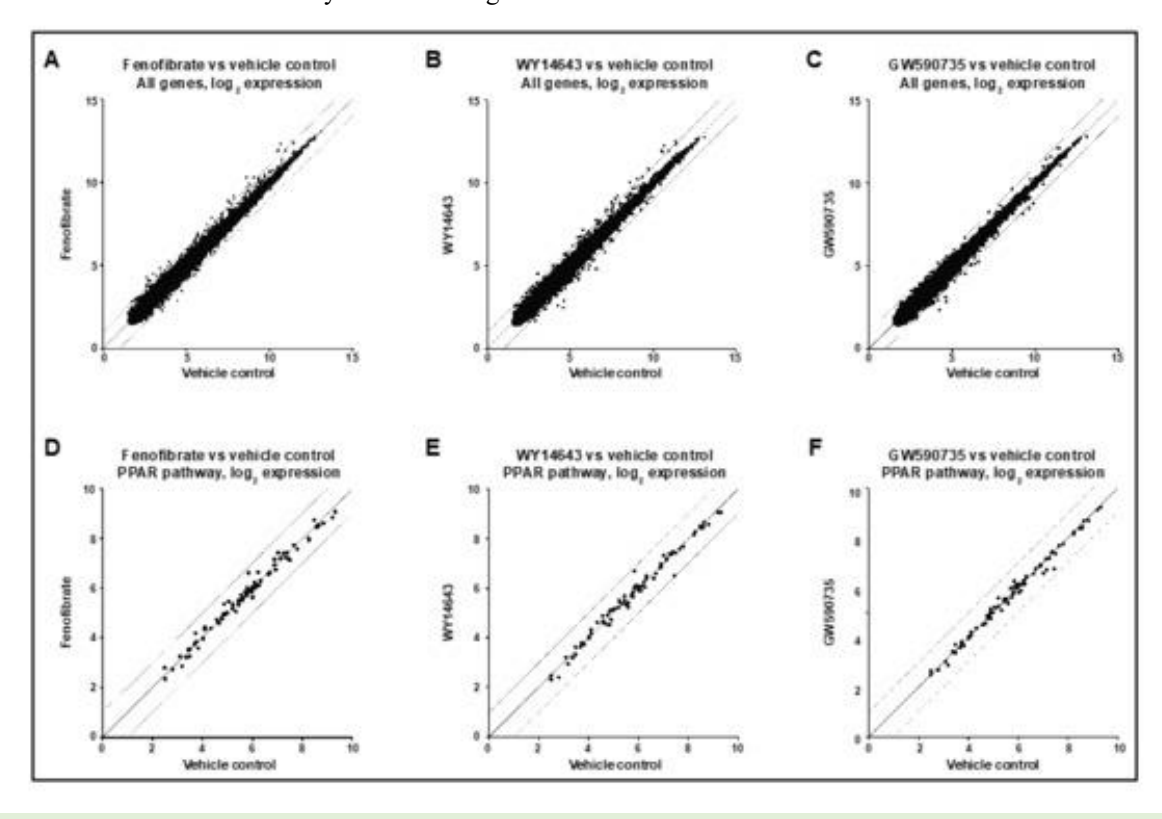


Figure 4. Intravitreous Fenofibrate and PPARα Agonists Do Not Change Retinal Gene Expression

Three-month-old male mice received intravitreal injections in both eyes with either fenofibrate, GW590735, WY14643, or a vehicle control (n = 3 per group). Retinas were collected 24 hours later, RNA was extracted and amplified, and global transcript levels were measured using microarrays. Panels A–C display log2-transformed expression values for all probes comparing treated versus control animals for fenofibrate, GW590735, and WY14643, respectively. Panels D–F focus on genes associated with the PPAR pathway (KEGG annotation). The solid diagonal line indicates identical expression between groups, while dashed lines denote a two-fold difference in expression. Across all treatments, no meaningful deviations from baseline were observed.

Oral fenofibrate does not activate PPARa targets in müller glia

Because rod photoreceptors dominate the whole retina, assessing PPAR α activity in less abundant cell types such as Müller glia requires targeted enrichment. To examine

this, Müller glia were isolated from GLAST-CreER+; R26CL:tdTomato fl/fl mice, in which tamoxifen triggers stable tdTomato expression specifically in glial cells. Cells were dissociated and sorted by fluorescence-activated cell sorting (FACS) to obtain a purified Müller glia population. Enrichment was confirmed by comparing GLAST-CreER+; R26CL:tdTomato fl/fl mice with Cre-negative littermates. Tamoxifen was administered between 1-2 months of age, and retinas were collected at six months. tdTomato fluorescence in frozen sections confirmed labeling restricted to Müller glia in Cre(+) mice, with no signal in Cre(-) controls (Figure 5A, B). FACS successfully separated a red fluorescent Müller glia population from non-fluorescent cells (Figure 5C). qPCR analysis demonstrated reduced rhodopsin transcript levels in the tdTomato+ population, indicating effective depletion of rod photoreceptors, along with increased expression of the Müller cell marker glutamine synthetase, confirming enrichment (Figure 5D).

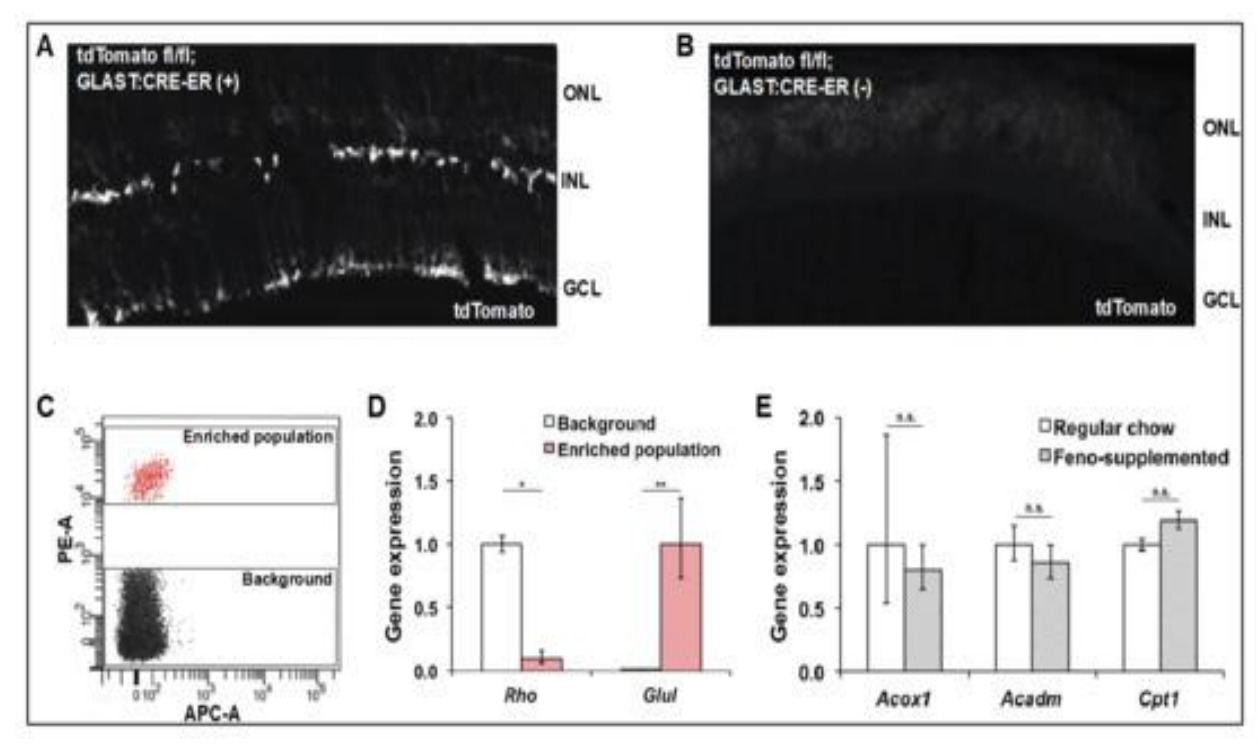


Figure 5. PPARα target genes are not upregulated in Müller glia from mice on a fenofibrate-supplemented diet. (A) Tamoxifen induction in GLAST-CreER; R26CL-tdTomato transgenic mice results in strong tdTomato expression specifically in Müller glia. (B) In contrast, mice lacking the GLAST-CreER transgene show no tdTomato expression in the retina. (C) GLAST-CreER; R26CL-tdTomato fl/fl mice were fed either a fenofibrate-enriched diet or standard chow beginning at one month of age and then induced with tamoxifen. At six months, retinas were collected, dissociated, and tdTomato-positive cells were isolated using fluorescence-activated cell sorting (FACS). (D) The sorted cell population was depleted of the rod marker rhodopsin and enriched for the Müller glia marker glutamine synthetase (n = 4, Student's t-test). (E) qPCR analysis revealed no changes in the expression of PPARα target genes—Acox1, Acadm, and Cpt1a—between Müller glia from mice on fenofibrate diet versus regular chow (n = 3, Student's t-test). ONL: outer nuclear layer; INL: inner nuclear layer; GCL: ganglion cell layer. * p < 0.05, ** p < 0.01

To assess the impact of oral fenofibrate on Müller glia gene expression, GLAST-CreER+; R26CL:tdTomato fl/fl mice were maintained on either standard chow or a fenofibrate-supplemented diet, with tamoxifen induction performed at 1-2 months of age. At six months, retinas were harvested, and Müller cell-enriched populations were isolated using FACS. Expression of canonical PPAR α target genes (Acox1, Acadm, and Cpt1) was not elevated in fenofibrate-treated mice, as determined by qPCR (Figure 5E), indicating that oral fenofibrate does not activate PPAR α in Müller glia under non-diabetic conditions.

Systemic or Local PPARa agonist administration activates a PPRE-Luciferase reporter in liver but not retina



To further investigate retinal responsiveness to PPAR α agonists, a luciferase reporter assay was performed to measure PPAR α activity in both retina and liver following treatment with the selective agonist GW590735. Transgenic mice carrying a PPRE-luciferase reporter received either intraperitoneal (IP) injections of GW590735 (10 mg/kg) or vehicle at three months of age (Figure 6A). Retinas collected 24 hours later showed no induction of luciferase activity (Figure 6B). Likewise, intravitreal injection of GW590735 (1 μ L, 500 nM in DMSO/NS 50:50) failed to activate the reporter in retinal tissue (Figure 6B). In contrast, liver tissue from IP-treated mice exhibited strong luciferase induction, confirming robust PPAR α activation in this organ (Figure 6B).

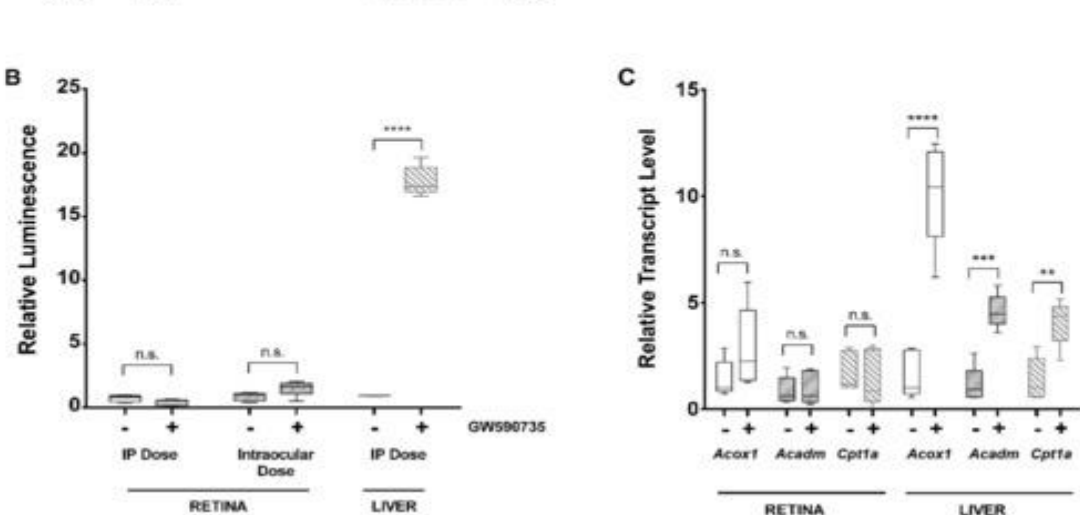


Figure 6. PPARα activation occurs in liver but not retina following systemic or local agonist administration.

To monitor tissue-specific PPAR α activity, a luciferase reporter construct was employed, comprising five consecutive peroxisome proliferator response elements (PPREs) upstream of a minimal thymidine kinase (TK) promoter, driving nuclear-targeted firefly luciferase, and flanked by 5' and 3' matrix attachment regions (MARs) (A). Luminescence was measured in retina and liver collected from six-month-old mice treated with the PPAR α agonist GW590735 (B). Administration of GW590735, either via intraperitoneal injection (10 mg/kg) or intravitreal delivery (2 μ L of 500 nM), failed to induce luciferase activity in the retina, whereas the liver showed strong reporter activation following systemic delivery (C). Concordantly, qPCR analysis revealed that IP GW590735 significantly increased expression of canonical PPAR α target genes—Acox1, Acadm, and Cpt1a—in liver tissue but produced no detectable changes in retinal tissue (n = 5 per group; two-way ANOVA with Bonferroni correction: ** p < 0.01, *** p < 0.001, **** p < 0.0001).

Further assessment of endogenous PPAR α targets confirmed these observations. Quantitative PCR of retina and liver after IP GW590735 administration demonstrated that Acox1, Acadm, and Cpt1a remained unchanged in retinal tissue, whereas all three genes exhibited 5- to 10-fold upregulation in the liver (**Figure 6C**). Together with the luciferase reporter results, these data indicate that GW590735 robustly activates PPAR α signaling in hepatic tissue but is ineffective in stimulating this pathway in the retina of non-diabetic mice.

Discussion

Our findings demonstrate that oral fenofibrate modulates metabolic and retinal physiology in a mouse model of type 2 diabetes, including improvements in circulating lipid profiles, attenuation of gliosis, and normalization of ERG abnormalities. These results align with observations in other diabetic models (type 1 and type 2) and in studies of retinopathy of prematurity [8-10, 15, 17, 34, 35],

supporting the continued investigation of fenofibrate as a therapeutic option for diabetic retinopathy. Models of type 2 diabetes, such as db/db mice or high-fat diet-induced models, may be particularly informative, as they replicate key pathophysiological features observed in the majority of human patients with diabetes.

The ERG alterations detected in this study—including delayed oscillatory potential implicit times and reduced b-wave amplitudes—point to dysfunction within the inner retina. Similar ERG changes have been reported in human diabetic retinopathy and are detectable before visible vascular alterations in both mice and humans [8, 26, 36], suggesting that neurodegeneration precedes vascular compromise. Advances in cell isolation and high-throughput sequencing techniques may soon enable detailed characterization of cell type-specific alterations within the inner retina, including Müller glia, vascular endothelial cells, pericytes, and the diverse neuronal populations such as amacrine, horizontal, bipolar, and ganglion cells.

Previous studies have indicated that PPARa signaling within the retina is critical for fenofibrate's protective effects [13-15]. Against this backdrop, our sequencing results showing that oral fenofibrate failed to upregulate PPARα target genes in the retina or Müller glia were unexpected. Complementing this, our luciferase reporter experiments demonstrated that retinal PPARa activity remained at baseline, whereas liver PPARα was strongly activated following oral fenofibrate. Comparable observations have been made in models of oxygeninduced retinopathy (OIR), where fibrate treatment enhanced PPARa target gene expression in the liver but not in the retina [37]. These findings suggest that, in patients with diabetic retinopathy, oral fenofibrate may primarily act on the liver, which could underlie the protective effects observed in the FIELD and ACCORD clinical trials [5, 6]. While these experiments were conducted in non-diabetic mice, and it remains possible that retinal PPARa activation occurs under diabetic conditions, the pronounced liver response alongside the lack of retinal induction indicates that the liver is likely the main site of fenofibrate action.

We hypothesize that fenofibrate's retinal benefits are mediated indirectly through systemic effects originating from the liver, rather than by direct retinal PPAR α activation. Fenofibrate has been reported to reduce diabetes-associated elevations of circulating IL-1 β , TNF α , VEGF, and Lp-LPA2 in patients [38]. In diabetic mouse models, fenofibrate increased serum Fgf21, which in turn promoted local upregulation of oxidative stress response genes in the retina and kidney [37, 39]. Such circulating factors may drive the fenofibrate-induced modulation of retinal inflammation, apoptosis, and oxidative stress-related genes documented in previous studies [17, 34, 35].

In conclusion, our data indicate that fenofibrate influences multiple aspects of db/db mouse phenotypes, including circulating triglycerides and cholesterol levels, retinal gliosis, and ERG parameters. While PPAR α target gene expression was not elevated in the retina or Müller glia, robust activation occurred in the liver. Collectively, these findings support the concept that fenofibrate exerts a protective effect in diabetic retinopathy, potentially through hepatic PPAR α activation rather than direct retinal engagement.

Acknowledgments: None.

Conflict of interest: None.

Financial support: None.

Ethics statement: None.

References

- 1. Lee R, Wong TY, Sabanayagam C. Epidemiology of diabetic retinopathy, diabetic macular edema and related vision loss. Eye Vis (Lond). 2015;2:17.
- Martinez-Zapata MJ, Martí-Carvajal AJ, Solà I, Pijoán J, Buil-Calvo J. Anti-vascular endothelial growth factor for proliferative diabetic retinopathy. Cochrane Database Syst Rev. 2014;(11):CD008721.
- Virgili G, Parravano M, Evans JR, Gordon I, Lucenteforte E. Anti-vascular endothelial growth factor for diabetic macular oedema: A network metaanalysis. Cochrane Database Syst Rev. 2018;(10):CD007419.
- Evans JR, Michelessi M, Virgili G. Laser photocoagulation for proliferative diabetic retinopathy. Cochrane Database Syst Rev. 2014;(11):CD011234.
- 5. Chew EY, Ambrosius WT, Davis MD, Danis RP, Gangaputra S, Greven CM, et al. Effects of medical therapies on retinopathy progression in type 2 diabetes. N Engl J Med. 2010;363(3):233-44.
- Keech A, Mitchell P, Summanen P, O'Day J, Davis TM, Moffitt MS, et al. Effect of fenofibrate on the need for laser treatment for diabetic retinopathy (FIELD study): A randomised controlled trial. Lancet. 2007;370(9600):1687-97.
- Srinivasan S, Hande P, Shetty J, Murali S. Efficiency of fenofibrate in facilitating the reduction of central macular thickness in diabetic macular edema. Indian J Ophthalmol. 2018;66(1):98-105.
- Pearsall EA, Cheng R, Matsuzaki S, Zhou K, Ding L, Ahn B, et al. Neuroprotective effects of PPARα in retinopathy of type 1 diabetes. PLoS One. 2019;14(4):e0208399.

- Shao Y, Chen J, Dong L, He X, Cheng R, Zhou K, et al. Protective effect of PPARα in endothelial progenitor cells through regulating metabolism. Diabetes. 2019;68(11):2131-42.
- Bogdanov P, Hernández C, Corraliza L, Carvalho AR, Simó R. Effect of fenofibrate on retinal neurodegeneration in an experimental model of type 2 diabetes. Acta Diabetol. 2015;52(1):113-22.
- 11. Hu Y, Chen Y, Ding L, He X, Takahashi Y, Gao Y, et al. Pathogenic role of diabetes-induced PPAR-α downregulation in microvascular dysfunction. Proc Natl Acad Sci U S A. 2013;110(38):15401-6.
- 12. Pearsall EA, Cheng R, Zhou K, Takahashi Y, Matlock HG, Vadvalkar SS, et al. PPARα is essential for retinal lipid metabolism and neuronal survival. BMC Biol. 2017;15(1):113.
- 13. Ding L, Cheng R, Hu Y, Takahashi Y, Jenkins AJ, Keech AC, et al. Peroxisome proliferator-activated receptor α protects capillary pericytes in the retina. Am J Pathol. 2014;184(10):2709-20.
- 14. Moran E, Ding L, Wang Z, Cheng R, Chen Q, Moore R, et al. Protective and antioxidant effects of PPARα in the ischemic retina. Invest Ophthalmol Vis Sci. 2014;55(7):4568-76.
- 15. Chen Y, Hu Y, Lin M, Jenkins AJ, Keech C, Mott R, et al. Therapeutic effects of PPARα agonists on diabetic retinopathy in type 1 diabetes models. Diabetes. 2013;62(1):261-72.
- 16. Li Q, Puro DG. Diabetes-induced dysfunction of the glutamate transporter in retinal Müller cells. Invest Ophthalmol Vis Sci. 2002;43(10):3109-16.
- 17. Liu Q, Zhang F, Zhang X, Cheng R, Ma J, Yi J, et al. Fenofibrate ameliorates diabetic retinopathy by modulating Nrf2 signaling and NLRP3 inflammasome activation. Mol Cell Biochem. 2018;445(1-2):105-15.
- 18. Mizutani M, Gerhardinger C, Lorenzi M. Müller cell changes in human diabetic retinopathy. Diabetes. 1998;47(3):445-9.
- Zong H, Ward M, Madden A, Yong PH, Limb GA, Curtis TM, et al. Hyperglycaemia-induced proinflammatory responses by retinal Müller glia are regulated by RAGE. Diabetologia. 2010;53(12):2656-66.
- Madisen L, Zwingman TA, Sunkin SM, Oh SW, Zariwala HA, Gu H, et al. A robust and highthroughput Cre reporting and characterization system for the whole mouse brain. Nat Neurosci. 2010;13(1):133-40.
- Mori T, Tanaka K, Buffo A, Wurst W, Kühn R, Götz M. Inducible gene deletion in astroglia and radial glia: A valuable tool for functional and lineage analysis. Glia. 2006;54(1):21-34.

- 22. Chen H, Charlat O, Tartaglia L, Woolf E, Weng X, Ellis SJ, et al. Evidence that the diabetes gene encodes the leptin receptor: Identification of a mutation in the leptin receptor gene in db/db mice. Cell. 1996;84(3):491-5.
- Biserni A, Giannessi F, Sciarroni AF, Milazzo FM, Maggi A, Ciana P. In vivo imaging reveals selective peroxisome proliferator activated receptor modulator activity of the synthetic ligand MK-886. Mol Pharmacol. 2008;73(5):1434-43.
- 24. Ciana P, Di Luccio G, Belcredito S, Pollio G, Vegeto E, Tatangelo L, et al. Engineering of a mouse for the in vivo profiling of estrogen receptor activity. Mol Endocrinol. 2001;15(7):1104-13.
- Oosterveer MH, Grefhorst A, Van Dijk TH, Havinga R, Staels B, Kuipers F, et al. Fenofibrate simultaneously induces hepatic fatty acid oxidation, synthesis, and elongation in mice. J Biol Chem. 2009;284(49):34036-44.
- 26. Rajagopal R, Bligard GW, Zhang S, Yin L, Lukasiewicz PD, Semenkovich CF. Functional deficits precede structural lesions in mice with high-fat diet-induced diabetic retinopathy. Diabetes. 2016;65(4):1072-84.
- Dobin A, Davis CA, Schlesinger F, Drenkow J,
 Zaleski C, Jha S, et al. STAR: Ultrafast universal RNA-seq aligner. Bioinformatics. 2013;29(1):15-21.
- 28. Liao Y, Smyth GK, Shi W. featureCounts: An efficient general purpose program for assigning sequence reads to genomic features. Bioinformatics. 2014;30(7):923-30.
- Wang L, Wang S, Li W. RSeQC: Quality control of RNA-seq experiments. Bioinformatics. 2012;28(16):2184-5.
- 30. Anders S, Huber W. Differential expression analysis for sequence count data. Genome Biol. 2010;11(10):R106.
- 31. Rajaratnam VS, Kai SE, Penn JS. Expression of peroxisome proliferator activated receptors (PPAR) alpha, beta and gamma and their angiostatic effects in a rat model of retinopathy of prematurity. Invest Ophthalmol Vis Sci. 2002;43(12):3717.
- 32. Enright JM, Lawrence K, Hadžić T, Corbo JC. Transcriptome profiling of developing photoreceptor subtypes reveals candidate genes involved in avian photoreceptor diversification. J Comp Neurol. 2015;523(4):649-68.
- 33. Kobayashi K, Forte TM, Taniguchi S, Ishida BY, Oka K, Chan L. The db/db mouse, a model for diabetic dyslipidemia: Molecular characterization and effects of Western diet feeding. Metabolism. 2000;49(1):22-31.
- 34. Liu Q, Zhang X, Cheng R, Ma J, Yi J, Li J. Salutary effect of fenofibrate on type 1 diabetic retinopathy

- via inhibiting oxidative stress-mediated Wnt/ β -catenin pathway activation. Cell Tissue Res. 2019;376(1):165-77.
- 35. Wang N, Zou C, Zhao S, Wang Y, Han C, Zheng Z. Fenofibrate exerts protective effects in diabetic retinopathy via inhibition of the ANGPTL3 pathway. Invest Ophthalmol Vis Sci. 2018;59(10):4210-7.
- 36. Tzekov R, Arden GB. The electroretinogram in diabetic retinopathy. Surv Ophthalmol. 1999;44(1):53-60.
- 37. Tomita Y, Ozawa N, Miwa Y, Ishida A, Ohta M, Tsubota K, et al. Pemafibrate prevents retinal pathological neovascularization by increasing FGF21 level in a murine oxygen-induced retinopathy model. Int J Mol Sci. 2019;20(23):5878.
- 38. Ju HB, Zhang FX, Wang S, Song J, Cui T, Li LF, et al. Effects of fenofibrate on inflammatory cytokines in diabetic retinopathy patients. Medicine (Baltimore). 2017;96(2):e7671.
- 39. Cheng Y, Zhang J, Guo W, Li F, Sun W, Chen J, et al. Up-regulation of Nrf2 is involved in FGF21-mediated fenofibrate protection against type 1 diabetic nephropathy. Free Radic Biol Med. 2016;93:94-109.